ADVANCED FUNCTIONAL MATERIALS

FULL PAPER

DOI: 10.1002/adfm.200500901

Orange and Red Organic Light-Emitting Devices Employing Neutral Ru(II) Emitters: Rational Design and Prospects for Color Tuning**

By *Yung-Liang Tung*, *Li-Shiuan Chen*, *Yun Chi*,* *Pi-Tai Chou*,* *Yi-Ming Cheng*, *Elise Y. Li*, *Gene-Hsiang Lee*, *Ching-Fong Shu*,* *Fang-Iy Wu*, and *Arthur J. Carty**

A new series of charge-neutral Ru(II) pyridyl and isoquinoline pyrazolate complexes, $[Ru(bppz)_2(PPh_2Me)_2]$ (bbpz: 3-*tert*-butyl-5-pyridyl pyrazolate) (**1**), $[Ru(fppz)_2(PPh_2Me)_2]$ (fppz: 3-trifluoromethyl-5-pyridyl pyrazolate) (**2**), $[Ru(ibpz)_2(PPhMe_2)_2]$ (ibpz: 3-*tert*-butyl-5-(1-isoquinolyl) pyrazolate) (**3**), $[Ru(ibpz)_2(PPh_2Me)_2]$ (**4**), $[Ru(ifpz)_2(PPh_2Me)_2]$ (ifpz: 3-trifluoromethyl-5-(1-isoquinolyl) pyrazolate) (**5**), [Ru(ibpz)$_2$(dpp=)] (dpp= represents *cis*-1,2-bis-(diphenylphosphino)ethene) (**6**), and [Ru(ifpz)$_2$(dpp=)] (**7**), have been synthesized, and their structural, electrochemical, and photophysical properties have been characterized. A comprehensive time-dependant density functional theory (TDDFT) approach has been used to assign the observed electronic transitions to specific frontier orbital configurations. A multilayer organic light-emitting device (OLED) using 24 wt % of **5** as the dopant emitter in a 4,4′-*N*,*N*′-dicarbazolyl-1,1′-biphenyl (CBP) host with 4,4′-bis[*N*-(1-naphthyl)-*N*-phenylamino]biphenyl (NPB) as the hole-transport layer exhibits saturated red emission with an external quantum efficiency (EQE) of 5.10 %, luminous efficiency of 5.74 cd A^{-1}, and power efficiency of 2.62 lm W^{-1}. The incorporation of a thin layer of poly(styrene sulfonate)-doped poly(3,4-ethylenedioxythiophene) (PEDOT) between indium tin oxide (ITO) and NPB gave anoptimized device with an EQE of 7.03 %, luminous efficiency of 8.02 cd A^{-1}, and power efficiency of 2.74 lm W^{-1} at 20 mA cm^{-2}. These values represent a breakthrough in the field of OLEDs using less expensive Ru(II) metal complexes. The nonionic nature of the complexes as well as their high emission quantum efficiencies and short radiative lifetimes are believed to be the key factors enabling this unprecedented achievement. The prospects for color tuning based on Ru(II) complexes are also discussed in light of some theoretical calculations.

1. Introduction

The development of new light-emitting materials has attracted great attention ever since the seminal study on organic electroluminescent (EL) devices by Tang and Vanslyke.[1] Researchers have been quite optimistic that organic light-emitting devices (OLEDs) will eventually provide an alternative to inorganic light-emitting diodes (LEDs) and liquid crystal displays (LCDs), perhaps affording brighter and more flexible displays at a lower cost.[2] In this context, the fabrication of OLEDs with efficient and saturated red emission is quite essential.[3] This has been achieved in part by using third-row phosphorescent dopant emitters, such as Os(II),[4] Ir(III),[5] and Pt(II),[6] where the strong spin-orbit coupling effectively promotes singlet-to-triplet intersystem crossing, as well as enhances the subsequent transition from the triplet to the ground state. Theoretically, OLEDs with 100 % internal quantum efficiencies could possibly be obtained by harnessing both the triplet and singlet excitons.[7] Despite these advantages, a major obstacle to the commercialization of phosphorescent OLED technologies lies in the prohibitive cost of the noble metals. From a technological perspective, there is an urgent need to develop phosphorescent emitting materials from less expensive precursors.

Amongst the numerous possible alternatives to precious metals that have been evaluated, the cationic tris-substituted Ru(II) bipyridine complex, $[Ru(bpy)_3]X_2$ (where X is a counterion such as ClO_4^- or BF_4^-, bpy: 2,2′-bipyridine), and its functionalized derivatives have attracted much attention.[8] These Ru(II) complexes have been used in solid-state light-emitting

[*] Prof. Y. Chi, Dr. Y.-L. Tung, L.-S. Chen
Department of Chemistry
National Tsing Hua University
Hsinchu 300 (Taiwan)
E-mail: ychi@mx.nthu.edu.tw
Prof. P.-T. Chou, Dr. Y.-M. Cheng, E. Y. Li, G.-H. Lee
Department of Chemistry and Instrumentation Center
National Taiwan University
Taipei 106 (Taiwan)
E-mail: chop@ntu.edu.tw
Prof. C.-F. Shu, F.-I. Wu
Department of Applied Chemistry
National Chiao Tung University
Hsinchu 300 (Taiwan)
E-mail: shu@cc.nctu.edu.tw
Prof. A. J. Carty
Steacie Institute for Molecular Sciences
National Research Council
Ottawa, ON K1A 0R6 (Canada)
E-mail: acarty@pco-bcp.gc.ca

[**] We acknowledge support from the following grants: 94-EC-17-A-08-S1-042, NSC 93-2113-M-007-012, and NSC 93-ET-7-007-003. Supporting Information is available online from Wiley InterScience or from the author.

electrochemical cells (LECs),[9] where the emissive layer contains an excess of mobile counterions and the charge injection is relatively independent of the nature of the contacts. As a result, light emission occurs through electrochemical redox processes, but requires a relatively long response time to reach the steady-state radiance.[9] In contrast, the fabrication of related polymer light-emitting devices (PLEDs) containing cationic Ru(II) dopant emitters has also been attempted,[10] and these are characterized by instantaneous light output, as compared to the LECs. Unfortunately, these cationic Ru(II) complexes are quite unsuitable for the fabrication of high-efficiency OLEDs using versatile vacuum deposition techniques. This can be mainly attributed to the poor volatility of these compounds, caused by their ionic nature, which leads to severe thermal degradation during evaporation. Furthermore, the ion-pair structure hampers the charge-transport efficiency. As a result, these Ru(II)-based PLEDs show a significantly inferior performance,[11] as compared to OLEDs doped with Os(II), Pt(II), and Ir(III) heavy-metal compounds.

This current situation makes the design and preparation of highly efficient Ru(II)-based emitters a daunting research challenge. In a recent short communication, we have unveiled our preliminary experimental data on the feasibility of fabricating an OLED based on a Ru(II) isoquinoline pyrazolate complex, $[Ru(ifpz)_2(PPh_2Me)_2]$ (ifpz: 3-trifluoromethyl-5-(1-isoquinolyl) pyrazolate).[12] However, identifying suitable analogues that can be used for the fabrication of Ru(II) OLEDs is non trivial. From a rational design perspective, the key to a suitable Ru(II) complex lies in the complete optimization of several crucial factors. A first requirement is that only charge-neutral Ru(II) complexes can be used; this is because of the stringent volatility and charge mobility criteria that need to be fulfilled for fabricating OLEDs. Secondly, the weaker ligand field strength for the second row congeners leads inevitably to the use of strongly bonding bidentate ligands, so that both the stability and the spin-orbit coupling can be greatly enhanced for the Ru(II) complexes (as discussed later). Thirdly, strong-field ancillary ligands, such as phosphines, are required to increase the energy gap of the metal centered *d*–*d* transition, so that the radiationless deactivation associated with metal–metal and/or metal–ligand stretching vibrations can be significantly suppressed.[13] Last but not least, the relatively high oxidation potential of Ru(II) necessitates the strategic design of ligand chromophores, particularly for color tuning, which is significantly different from established strategies for designing ligands for third-row transition metals (as discussed below).

In this study, we report the first comprehensive synthesis of seven charge-neutral Ru(II) pyridyl and isoquinoline pyrazolate complexes, $[Ru(bppz)_2(PPh_2Me)_2]$ (bppz: 3-*tert*-butyl-5-pyridyl pyrazolate) (**1**), $[Ru(fppz)_2(PPh_2Me)_2]$ (fppz: 3-trifluoromethyl-5-pyridyl pyrazolate) (**2**), $[Ru(ibpz)_2(PPh_2Me)_2]$ (ibpz: 3-*tert*-butyl-5-(1-isoquinolyl) pyrazolate) (**3**), $[Ru(ibpz)_2(PPh_2Me)_2]$ (**4**), $[Ru(ifpz)_2(PPh_2Me)_2]$ (**5**), $[Ru(ibpz)_2(dpp{=})]$ (dpp= represents *cis*-1,2-bis-(diphenylphosphino)ethene (**6**), and $[Ru(ifpz)_2(dpp{=})]$ (**7**), the structures of which are depicted in Scheme 1.

We have investigated the basic electrochemical and photophysical properties of these molecules and explored their feasibility for OLED applications. Moreover, we have carried out theoretical studies of these Ru(II) complexes, which provide additional insight into their electronic transitions and the frontier orbital configurations involves in these transitions. The results suggest a method for generating red light emission and uncover a surprising electronic aspect of the relative ligand orientation. Accordingly, we also discuss the fundamental basis for color tuning in OLEDs based on these Ru(II) complexes.

2. Results and Discussion

2.1. Synthesis and Structural Characterization

2-Pyridyl pyrazole-type ((pypz)H) chelate ligands can readily react with main group metal[14] and transition metal reagents,[15] affording the corresponding chelate complexes in high yields. A similar synthetic strategy has been utilized to prepare osmium-based complexes, such as $[Os(CO)_2(pypz)_2]$, by the direct treatment of the free ligand with $Os_3(CO)_{12}$ in a

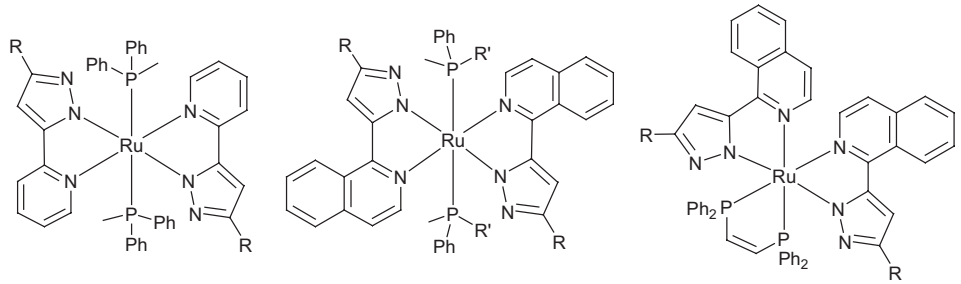

R = ^{t}Bu, (**1**)

R = CF_3, (**2**)

R = ^{t}Bu, R' = Me, (**3**)

R = ^{t}Bu, R' = Ph, (**4**)

R = CF_3, R' = Ph, (**5**)

R = ^{t}Bu, (**6**)

R = CF_3, (**7**)

Scheme 1. Relevant structural drawings for ruthenium complexes **1**–**7**.

ADVANCED FUNCTIONAL MATERIALS

stainless-steel autoclave at high temperature.[16] The overall transformation can be written as

$$6\,(pypz)H + Os_3(CO)_{12} \rightarrow 3\,[Os(CO)_2(pypz)_2] + 3H_2 + 6\,CO \quad (1)$$

Moreover, simply treating the formed complex with a decarbonylation reagent, Me_3NO, followed by the addition of π-accepting phosphorus donors, leads to the isolation of related metal complexes $[Os(pypz)_2L_2]$ (L = PPh_2Me and $PPhMe_2$) in moderate yields.[17] It is notable that these osmium complexes exhibit bright and tunable orange-red to red phosphorescence both in solution and in the solid state at room temperature. Accordingly, these molecules can potentially be used as dopant emitters for practical OLED applications.

Attempts have been made to synthesize the second-row ruthenium analogues of **1**–**7**, the structures of which are shown in Scheme 1. The target Ru(II) emitting complexes have been prepared by the reaction of $Ru_3(CO)_{12}$ with 2-pyridyl or 1-isoquinolyl pyrazoles, followed by treatment with a phosphine in the presence of Me_3NO, giving complexes **1**–**5** in high yields (> 60 %). Alternatively, a second approach involves the heating of the pyrazole ligand with the phosphine complex $[Ru(CO)_3(dpp{=})]$ in the presence of Me_3NO, affording the dpp=-substituted light-emitting complexes **6** and **7** in good yields (ca. 60 %).

From a molecular design perspective, the introduction of dual pyrazolate anions neutralizes the 2+ charge on the central Ru(II) cation. Moreover, owing to the strong nucleophilic nature of the pyrazolate nitrogen, strong coordination to the ruthenium metal center is expected. It is notable that in the present work, the 2-pyridyl substituents in complexes **1** and **2** have been deliberately replaced by 1-isoquinolyl substituents, forming complexes **3**–**7**, in an attempt to raise the typically low highest occupied molecular orbital (HOMO) energy level at the Ru(II) metal center, thereby generating the required saturated red emission. Moreover, since the Franck–Condon factors for nonradiative transitions are qualitatively proportional to the square of the bond displacement,[18] the enlarged π-conjugation of the isoquinoline motif (vs. that of the pyridyl group) should lead to minimal structural deformation between the ground and excited states, as well as reduce the thermal population of the upper *d*–*d* excited states that generally dominate the nonradiative deactivation. Such ligand modifications should thus improve the emission quantum yields.

These ruthenium metal complexes exhibit good solubility and thermal stability in typical organic solvents, as evidenced by the negligible degradation in both the solid and solution phase over a period of several weeks. The only exception is complex **1**, which is originally orange in color, but turns dark green in $CHCl_3$ solution after 1–2 h in air. Nevertheless, the chemical stability of **1** could be enhanced by switching from chlorinated to nonchlorinated solvents. As a result, all NMR characterizations have been carried out in nonchlorinated solvents, such as deuterated benzene or acetone. Moreover, complexes **3** and **6** have been further characterized using single-crystal X-ray diffraction analysis to establish their exact 3D molecular architectures (Table 1).

Table 1. Crystal data and refinement parameters for complexes **3** and **6**.

Compound	**3**	**6**
Formula	$C_{48}H_{54}N_6P_2Ru$	$C_{58}H_{54}N_6P_2Ru$
Molecular weight	877.98	998.08
Crystal system	Triclinic	Monoclinic
Space group	*P*–1	$P2_1/n$
Crystal size [mm^3]	0.25 × 0.20 × 0.20	0.45 × 0.35 × 0.35
a [Å]	10.3625 (6)	14.8192 (6)
b [Å]	10.7786 (6)	17.0842 (7)
c [Å]	11.5824 (7)	19.9811 (8)
α [°]	101.765 (1)	
β [°]	102.792 (1)	91.1660 (10)
γ [°]	112.007 (1)	
V [$Å^3$]	1109.21 (11)	5057.7 (4)
Z	1	4
$\rho_{calc.}$ [g cm^{-3}]	1.314	1.311
Temperature [K]	295 (2)	295 (2)
μ [mm^{-1}]	0.465	0.417
Reflections collected	14741	49950
Independent reflections	5089 [*R*(int) = 0.0286]	11600 [*R*(int) = 0.0619]
R_F, $R_w(F^2)$ (all data)	0.0358, 0.0829	0.0771, 0.1211
R_F, $R_w(F^2)$ [$I > 2\sigma(I)$]	0.0332, 0.0810	0.0549, 0.1119
GOF	1.078	1.072

Figure 1 shows the molecular structure of the prototypical complex **3**. It is clear that the $PPhMe_2$ ligands lie in the expected trans configuration, with the isoquinolyl pyrazolate chelates occupying the remaining four planar positions around the central ruthenium atom. The Ru–N distances for these chelating bonds are similar to those observed for related cationic Ru(II) diimine complexes (2.042–2.079 Å).[19] Conversely, the Oak Ridge thermal ellipsoid plot (ORTEP) diagram of **6** reveals a cis arrangement, as prescribed by the dpp= chelate (Fig. 2). The ibpz chromophores adopt an eclipsed orientation

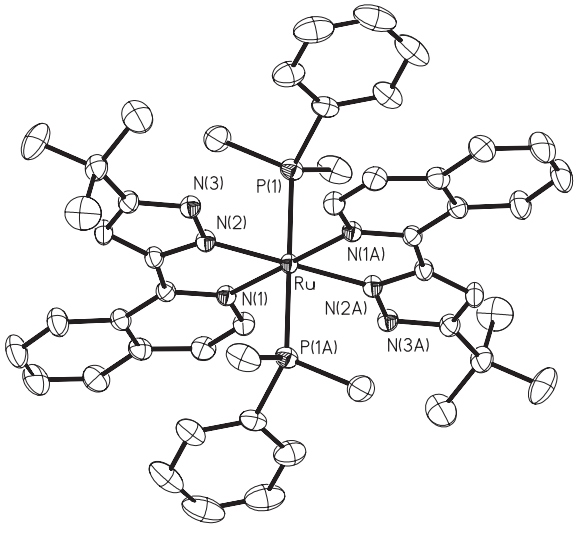

Figure 1. Oak Ridge thermal ellipsoid plot (ORTEP) diagram of **3** with thermal ellipsoids shown at the 25 % probability level; selected distances: Ru–N(1) = 2.0803(15) Å, Ru–N(2) = 2.0461(15) Å, and Ru–P(1) = 2.3240(5) Å; selected angles: N(1)–Ru–N(2) = 76.20(6)°, N(2)–Ru–P(1) = 89.88(5)°, and N(1)–Ru–P(1) = 89.21(4)°.

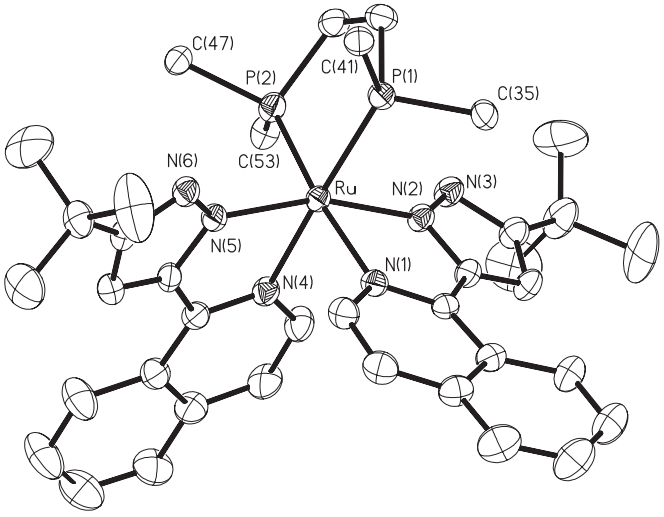

Figure 2. ORTEP diagram of **6** with thermal ellipsoids shown at the 30% probability level with the phenyl substituents of the dpp= ligand represented by their ipso-carbon for clarity; selected distances: Ru–N(1) = 2.136(2) Å, Ru–N(2) = 2.047(2) Å, Ru–N(4) = 2.128(2) Å, Ru–N(5) = 2.071(2) Å, Ru–P(1) = 2.2927(8) Å, and Ru–P(2) = 2.2575(9) Å; selected angles: N(1)–Ru–N(2) = 76.43(9)°, N(4)–Ru–N(5) = 75.79(9)°, N(2)–Ru–N(5) = 161.81(10)°, N(1)–Ru–P(2) = 173.27(7)°, N(4)–Ru–P(1) = 173.55(7)°, and P(2)–Ru–P(1) = 83.15(3)°.

with both the pyrazolate nitrogen atoms N(2) and N(5) aligned trans to each other, and with the isoquinolyl nitrogen atoms N(1) and N(4) located trans to the chelating phosphorus atoms. This change of coordination geometry notably improves the Ru–P bonding, leading to a reduction of the average Ru–P distance from 2.324 Å in **3** to 2.275 Å in **6**; this also causes an increase of the Ru–N(isoquinoline) bond distance from 2.080 Å in **3** to a much greater value of 2.132 Å in **6**, while leaving the *trans*-Ru–N(pyrazolate) distances essentially unaltered; 2.046 Å in **3** versus 2.059 Å in **6**. This variation in bonding is presumably caused by the much greater trans effect of the π-accepting phosphines. The weakened Ru–N(isoquinoline) bonding in **6** may induce relatively faster radiationless deactivation, as compared to the trans analogues described above, leading to a reduced phosphorescence quantum yield for the cis complexes.

2.2. Photophysical Measurements

The photophysical properties of these ruthenium complexes can be systematically tuned by modification of the pyrazolate chromophores and the ancillary phosphine ligands; the relevant data is shown in Table 2. In the UV-vis spectrum of **1**, the high-energy absorption bands at $\lambda \leq 360$ nm arise from intraligand π–π* transitions (Fig. 3). The next lower energy band, with λ_{max} at 395 nm, can be assigned to singlet metal–ligand charge transfer (MLCT), while the weak absorptions extending into the 443–493 nm region are associated with spin-forbidden triplet π–π* and MLCT transitions. The π–π* and MLCT transitions of **2** can be analogously assigned, showing a blue-shift because of the introduction of electron-withdrawing CF_3 substituents. For the trans isoquinolyl complexes **3–5**, the UV-vis spectra reveal strong absorption bands ($\varepsilon > 10^4$ M^{-1} cm^{-1}) in the ≤380 nm region, which can be reasonably assigned to spin-allowed ^{1}π–π* transitions in the ibpz (or ifpz) ligands. The next lower energy ^{1}MLCT absorption band appears around 450 nm, while the weak absorptions centered at 580 nm ($\varepsilon = 900$ M^{-1} cm^{-1}), 566 nm ($\varepsilon = 1100$ M^{-1} cm^{-1}), and 523 nm ($\varepsilon = 1000$ M^{-1} cm^{-1}) for complexes **3–5**, respectively, can reasonably be assigned to a mixed state involving both spin-orbit coupling enhanced ^{3}π–π* and ^{3}MLCT transitions. It is also notable that the CF_3 substituents in **5** not only cause a spectral blue-shift for the ^{1}π–π* and ^{1}MLCT absorptions but also increase the transition moment.

At room temperature, in the solution phase, independent of the solvents used, these complexes show rather poor emission quantum yields, ranging from the nonemissive behavior of **2** and a very low value of 0.1 % for **1** to a highest value of 1 % for **5** (Table 2). This behavior is in sharp contrast to osmium(II) analogues of these complexes, where bright phosphorescence emission can be clearly observed in the solution phase at room temperature.[17] This difference may arise from the lower excited-state energy gap. Thus, rapid quenching may occur in solution, possibly incorporating internal conversions through large amplitude motions and collisional deactivation. In addition, one should not neglect the relatively weaker bonding of the ligands to Ru(II), as compared to corresponding neutral Os(II) or Ir(III) complexes, which may result in a shallow potential energy surface along the stretching motions of the Ru–ligand bond, and thus may trigger a fast radiationless tran-

Table 2. Photophysical and electrochemical properties for complexes **1–7**.

	UV-vis absorption; in CH_2Cl_2; [nm] (ε) [a]	PL [a] λ_{max} [nm]	Φ [a]	τ_{obs} [μs]	$E_{1/2}^{ox}$	$E_{1/2}^{red}$
1	309 (18 600), 395 (10 300),	—	—	—	−0.24 [b]	
	443 (1400), ~493 (900, br)	(568)	(0.001)	(0.16)		
2	297 (21 800), 392 (11 700),	—	—	—	0.19 [b]	
	~460 (700, br)	—	—	—		
		[522, 650 (sh)]	—	[20.8]		
3	336 (20 200), 363 (13 700),	718	— (0.02)	—	−0.38	−2.67
	462 (12 500), ~580 (900, br)	(709)		(1.06)		
4	332 (19 800), 361 (14 600),	700	— (0.02)	—	−0.33	−2.64
	455 (12 200), ~566 (1100,	(683)	—	(0.64)		
	br)	[665]		[18.7]		
5	320 (24 600), 353 (12 900),	636	0.01 (0.24)	0.10	0.13	−2.50
	446 (17 300), ~523 (1000,	(632)	—	(1.82)		
	br)	[620]		[6.5]		
6	316 (23 200), 356 (19 700),	637	0.08 (0.21)	0.06	−0.23	−2.60
	368 (20 000), 408 (9000),	(609)	—	(2.1)		
	~470 (3900, br)	[600]		[19.6]		
7	307 (22 200), 345 (15 800),	596	0.002 (0.02)	0.02	0.36	−2.40
	359 (18 000), 390 (9600),	(571, 589)	—	(0.56)		
	~445 (3100, br)	[563, 594]		[37.8]		

[a] Samples were degassed and measured in CH_2Cl_2 solution at room temperature with ε in M^{-1} cm^{-1}. Data in parentheses are measured in the solid state at room temperature while the data in square brackets has been measured in a frozen CH_2Cl_2 matrix at 77 K. [b] Data recorded in THF solution.

ADVANCED FUNCTIONAL MATERIALS

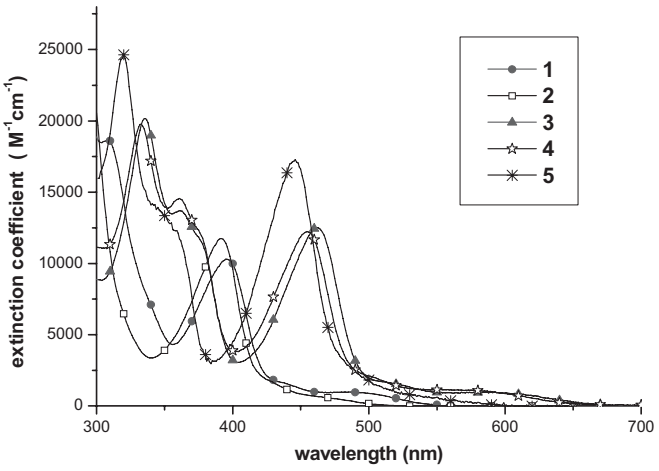

Figure 3. UV-vis absorption spectra of complexes **1**–**5** in CH_2Cl_2 at room temperature.

sition via the intercept (e.g., a conical interception) with the ground-state energy surface.[16] As for complexes **1** and **2**, the reduction of π-conjugation on the pyridyl motif not only causes a large structural deformation between the ground and excited states, but also possibly increases the thermal population of the upper *d*–*d* excited states which dominate the nonradiative deactivation processes. The details are discussed in a subsequent section on theoretical calculations.

In sharp contrast, moderate to highly intense luminescence is observed for the isoquniolyl complexes when they are vacuum deposited as thin solid films; the λ_{max} for the emission peak is located at 709, 683, and 632 nm, respectively for complexes **3**–**5** (Fig. 4). The partial overlap between these emission signals and the lowest energy absorption bands, along with the observed broad, structureless spectral features, leads us to conclude that the phosphorescence originates primarily from the ^{3}MLCT state.[20] Moreover, in comparison to the $PPhMe_2$ anchored complex **3**, the PPh_2Me derivative **4** exhibits an approximately 27 nm hypsochromic shift in λ_{max}, which can be

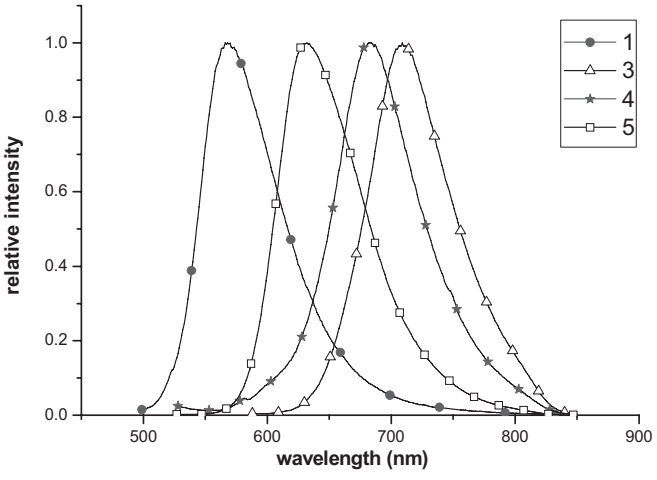

Figure 4. Normalized emission spectra of **1** (–●–), **3** (–△–), **4** (–★–), and **5** (–□–) as thin solid films at room temperature.

qualitatively rationalized by the lowering of the Ru(II) d_π energy level due to an increase in the π-accepting strength. For the ifpz complex **5**, an even more notable hypsochromic shift of 50 nm is observed. This is apparently caused by the electron-withdrawing effect of the CF_3 substituents on the pyrazolate ligand, which further lowers the electron charge density on the Ru(II) metal center, consequently raising the MLCT energy level. It is also noteworthy that the radiative lifetime of approximately 7.58 μs deduced for **5** from the observed lifetime (1.82 μs) and the phosphorescence quantum yield (0.24, Table 2) is similar in magnitude to values previously reported for efficient red-emitting Ir(III) complexes.[21] This result manifests the importance of using ibpz and ifpz ligands, which are able to greatly enhance the spin-orbit coupling, possibly due to the closer proximity between Ru(II) and the pyrazolate chromophores.

To obtain additional insights, the UV-vis spectra of the cis complexes **6** and **7** have been recorded and are depicted in Figure 5. It is worth noting that although the higher energy intraligand ^{1}π–π absorptions at ≤408 nm have almost the same intensity, the lower lying ^{1}MLCT transitions at 470 and 445 nm

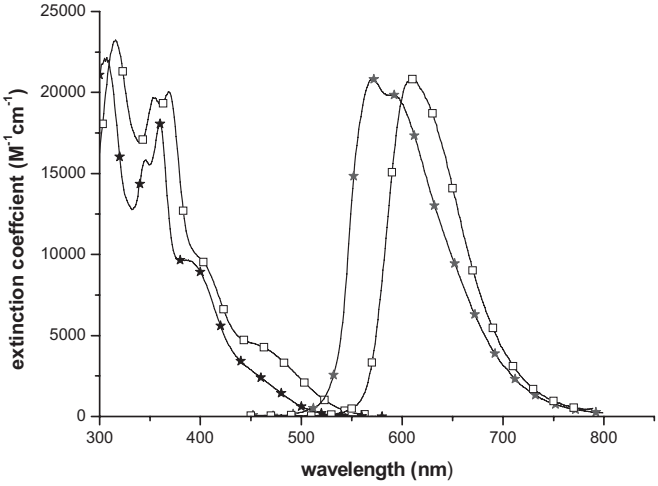

Figure 5. UV-vis absorption spectra of **6** (–□–) and **7** (–★–) in CH_2Cl_2 at room temperature and normalized emission spectra obtained for thin solid films of **6** and **7** (λ_{ex} = 450 nm).

for **6** and **7**, respectively, show a significant decrease in signal intensity and also exhibit extensive spectral overlaps with the triplet π–π* and MLCT transitions. The reduction of the ^{1}MLCT transition moment is tentatively ascribed to the cis-arranged, stronger π-accepting dpp= ligand, which significantly lowers the relative electron density at the central Ru(II) atom. The excitation of solid films of **6** and **7** at room temperature gives long-lived orange-red to red luminescence (see Table 2). For complex **7**, the blue-shift of the emission peak wavelength to 571 nm, as opposed to the 609 nm peak observed for **6**, is due to the electron-withdrawing CF_3 substituent on the ifpz ligands. Another notable feature of **7** is the gradual emergence of an intraligand ^{3}π–π* contribution, which is supported by the

occurrence of a second emission peak at $\lambda_{max} = 589$ nm, arising from the vibronic coupling.

Finally, in comparison to the data obtained at room temperature, a much longer phosphorescence lifetime, and thus an increased phosphorescence quantum yield, has been measured for complexes **4–7** in a frozen CH_2Cl_2 matrix at 77 K. These results indicate a dominant thermally activated radiationless process for all the complexes studied.

2.3. Electrochemistry

The redox potentials of the Ru(II) complexes have been determined from cyclic voltammograms, and the data are summarized in Table 2. It is believed that oxidation occurs mainly at the metal site, along with minor contributions from the pyrazolate chelates and phosphine ligands. This hypothesis is further corroborated by theoretical studies presented in a subsequent section. Accordingly, the bppz complex **1** shows an oxidation potential of –0.24 V, while the fppz complex **2** exhibits a higher oxidation potential of 0.19 V due to the presence of CF_3 substituents, which reduce the electron density at the metal atom. Similarly, replacing the electron-withdrawing CF_3 group on the chelate chromophores with an electron-donating *tert*-butyl moiety leads to a decrease of the oxidation potential, as demonstrated by the higher oxidation potential of **5** (0.13 V) versus that of **4** (–0.33 V), as well as by the decrease of the oxidation potential of **6** (–0.23 V) versus that of **7** (0.36 V). Moreover, comparing the oxidation potentials of a pair of complexes, **4** (–0.33 V) versus **6** (–0.23 V), and for another pair of complexes, **5** (0.13 V) versus **7** (0.36 V), reveals that a cis orientation induces a higher oxidation potential as compared to a trans orientation, assuming that the electronic effects of PPh_2Me are comparable to that of the chelating dpp= ligand. Finally, a comparison of the oxidation potentials of the two trans complexes **3** and **4** indicates that the π-accepting character of the phosphine ligands is slightly increased in the order $PPhMe_2 < PPh_2Me$.

As for the reduction behavior, except for the pyridyl pyrazolate complexes **1** and **2**, neither of which gives a visible reduction peak in tetrahydrofuran (THF) solution, the isoquinolyl complexes **3–7** exhibit reversible reduction signals in a narrow range between –2.40 and –2.67 V. The similar behavior of these complexes leads us to believe that the observed reduction is mainly associated with the isoquniolyl groups, while the ancillary phosphine π-acceptors and the substituents on the pyrazolate segments likely influence the electrochemical potential of the central metal atom. The reduction potentials shown in Table 2 are fully consistent with this delineation; however, the variation of the data is far less significant than that seen for the oxidative potentials. The lowest reduction potential (–2.40 V) observed for **7** is due to its electron-withdrawing CF_3 substituents and the more efficient π-accepting character of the dpp= ligand. It is worth noting that the redox cycle for compounds **3–7** is fully reversible even after >10 scans, indicating the superior redox stability of these complexes, which is a key requirement for OLED applications.

2.4. Fabrication of OLED Devices

Remarkably high emission efficiencies in the red have been obtained for OLED devices fabricated using vacuum deposition. Multilayer devices have been fabricated containing indium tin oxide (ITO), 4,4′-bis[*N*-(1-naphthyl)-*N*-phenylamino]-biphenyl (NPB), 4,4′-*N*,*N*′-dicarbazolyl-1,1′-biphenyl (CBP), 2,9-dimethyl-4,7-diphenyl-1,10-phenanthroline (BCP), and tris(8-hydroxyquinolinato) aluminum(III) (AlQ_3). The multilayer devices with a configuration of ITO/NPB (40 nm)/CBP:**5** (30 nm)/BCP (10 nm)/AlQ_3 (30 nm)/Mg:Ag (10:1) (50 nm) have been fabricated using various doping concentrations of **5**: 6, 12, 24, 50, and 100 %. The configuration used here is based on devices previously reported by Adachi et al.[22] The crucial device performance characteristics are summarized in Table 3.

Bright red emission is observed for all of the concentrations used, even when using a nondoped architecture. The current–voltage–luminance (*I–V–L*) curves plotted in Figure 6a reveal a trend of decreasing drive voltage with increasing doping levels, implying that the dopant may also serve to transport charge.[23] The EL spectra are depicted in Figure 6b; a small emission peak is seen at approximately 450 nm at low dopant concentrations of 6 and 12 %, and can be identified to originate from NPB. The NPB emission diminishes and became negligible upon increasing the doping concentration to 24 % and higher. Concurrently, a small red-shift of the EL spectra is observed with increasing dopant concentrations, λ_{max} is at approximately 624 nm for the 5 % device and shifts to 630 nm for the neat film device (Fig. 6b), presumably due to the change in the polarity of the medium.[24] Further optimization can be achieved by the incorporation of a thin layer of poly(styrene sulfonate)-doped poly(3,4-ethylenedioxythiophene) (PEDOT) to improve the surface smoothness and to serve as a hole injection layer.[25] The best results, with an external quantum efficiency (EQE) of 7.03 %, luminous efficiency of 8.02 cd A^{-1}, and power efficiency of 2.74 lm W^{-1}, have been obtained using this configuration at a current density of 20 mA cm^{-2}.

The decent performance of this series of devices can be plausibly attributed to the remarkably short radiative lifetime (~7.58 μs, as discussed above) for **5**, as well as to the existence of the two trans-oriented phosphine ligands, which effectively block the aromatic chromophores from significantly interacting in the solid state, thereby greatly reducing triplet–triplet annihilation. This, in combination with the electron deficient nature of the isoquinoline moiety (or its quinoline analogue), allows for more balanced charge injection, transportation, and recombination processes in the emissive layer.[26]

Moreover, it is important to note that complex **5** does not crystallize at doping concentrations ≤50 %, which is revealed by the minor variations in the luminescence efficiencies. Such an observation is consistent with a recent report on an iridium(III) emitter, wherein an EQE of 5.5 % was observed for a device using a 100 % concentration of the dopant,[27] suggesting that the films remained smooth and uniform under these conditions. However, for devices prepared using a 100 % concentration of **5**, the EQE drops from 5.1 to 2.1 %, which may

ADVANCED FUNCTIONAL MATERIALS

Table 3. Performance characteristics for the device configuration: ITO/NPB/CBP:X % Ru complexes/BCP/AlQ_3/Mg:Ag.

Concentration [%]	Maximum luminescence [a] [cd m^{-2}]	EQE [b][c] [%]	Lum. [b][c] [cd m^{-2}]	Luminous efficiency [b][c] [cd A^{-1}]	Power efficiency [b][c] [lm W^{-1}]	λ_{max} [nm] CIE (x, y) [d]	Turn-on voltage [e] [V]
			complex **5** as dopant emitter				
6%	8386 (16.0 V)	4.54 (3.21)	1086 (3845)	5.46 (3.86)	1.97 (1.08)	626/ (0.65, 0.33)	3.7
12%	9935 (16.0 V)	5.06 (3.66)	1174 (4223)	5.87 (4.24)	2.31 (1.29)	627/ (0.67, 0.33)	3.2
24%	10 079 (15.0 V)	5.10 (3.92)	1146 (4398)	5.74 (4.42)	2.62 (1.50)	630/ (0.67, 0.33)	3.0
50%	11 052 (15.0 V)	5.01 (4.46)	1076 (4442)	5.38 (4.45)	2.63 (1.60)	630/ (0.67, 0.33)	2.7
100%	6320 (12.5 V)	2.14 (1.92)	463 (2083)	2.32 (2.09)	1.42 (0.93)	630/ (0.67, 0.33)	2.7
			complex **5** as dopant with PEDOT–PSS as the hole injection layer				
24%	8822 (16.0 V)	7.03 (4.74)	1592 (5392)	8.02 (5.40)	2.74 (1.34)	628/ (0.67, 0.33)	3.0
50%	11 638 (16.0 V)	5.00 (4.07)	1235 (5023)	6.17 (5.03)	2.85 (1.63)	628/ (0.67, 0.33)	2.6
			complex **6** as dopant emitter				
12%	5572 (15.5 V)	2.30 (1.52)	820 (2719)	4.13 (2.73)	2.10 (0.99)	614/ (0.60, 0.39)	2.7

[a] Values in parentheses are the applied driving voltages. [b] Data collected using a current density of 20 mA cm^{-2}. [c] Values in parentheses represent data collected at a current density of 100 mA cm^{-2}. [d] Measured at a driving voltage of 8 V. [e] Data showing a brightness of 1 cd m^{-2}.

partially be caused by crystallite formation during device fabrication.

In order to investigate the EL performance versus the emitting material, we have fabricated similar OLED devices using the cis-orientated phosphine complex **6**, which is quite similar to **5** in terms of its emission wavelength and quantum yield in solution. Unfortunately, for an optimized multilayer device using 12 wt % of **6** as a dopant emitter, we observe a reduced maximum luminescence of 5572 cd m^{-2} at 15.5 V, and an EQE of 2.3 %, luminous efficiency of 4.13 cd A^{-1}, and power efficiency of 2.10 lm W^{-1} at a driving voltage of 20 mA cm^{-2}. Furthermore, the color chromaticity of this device also shifts from saturated red to red-orange with less desirable Commission Internationale de l'Eclairage (CIE) coordinates of (0.60, 0.39), which could be due to the slight blue-shifted emission at 609 nm in the solid state (see Table 2).

2.5. Upper Energy-Gap Limit for Efficient Ru(II) OLEDs

Once we have demonstrated the preparation of highly efficient, charge-neutral phosphorescent Ru(II) metal complexes and their corresponding OLEDs, the next critical challenge is to be able to tune the emission wavelength. The emission wavelength can be tuned by the systematic variation of the ancillary phosphines as well as by derivatization of the pyrazolate chromophores. However, given the high oxidation potential and relatively weak ligand-field strength of Ru(II), a fundamental question that naturally arises is how high in energy can the ^{3}MLCT or $^3\pi$–π^* transitions be tuned in these Ru(II) complexes before crossing over to the metal-centered d–d state,[13] which is widely accepted to be the main radiationless deactivation channel in nature due the weakened metal–ligand bond strength and forbidden transitions (from excited to ground states).

To better understand this underlying issue, we have performed theoretical calculations (time-dependent density functional theory (TDDFT), see experimental section) to model the photophysical properties of the prepared neutral Ru(II) complexes. Figure 7 depicts the features of selected occupied and unoccupied frontier orbitals primarily involved in the lower-lying transitions for complexes **2**, **3**, and **6**, while the descriptions and the energy gaps for each transition are listed in Table 4. The lowest singlet $S_0 \rightarrow S_1$ transitions for **3** and **6** are calculated to be at 615 and 504 nm, respectively, which is in good agreement with the values observed experimentally in the absorption spectra (**3**: 580 nm, **6**: 470 nm). Likewise, the estimated $S_0 \rightarrow T_1$ transition at 660 nm for **3** is qualitatively consistent with the observed 718 nm phosphorescence. The deviation of the current theoretical approach from the experimental results is mainly due to the experimental difficulties in determining the absorption peak frequency. The broad and diffusive nature of the $S_0 \rightarrow S_1$ peak causes a large uncertainty in determining the onset of emission. In addition, these discrepancies may partially be explained by the underestimation of the mixing of the high density of low lying states or the less-extensive basis set used for the Ru(II) atom. On the other hand, it is also unfair to compare the energy gap calculated for the $S_0 \rightarrow T_1$ transition in the gas phase to values obtained from phosphores-

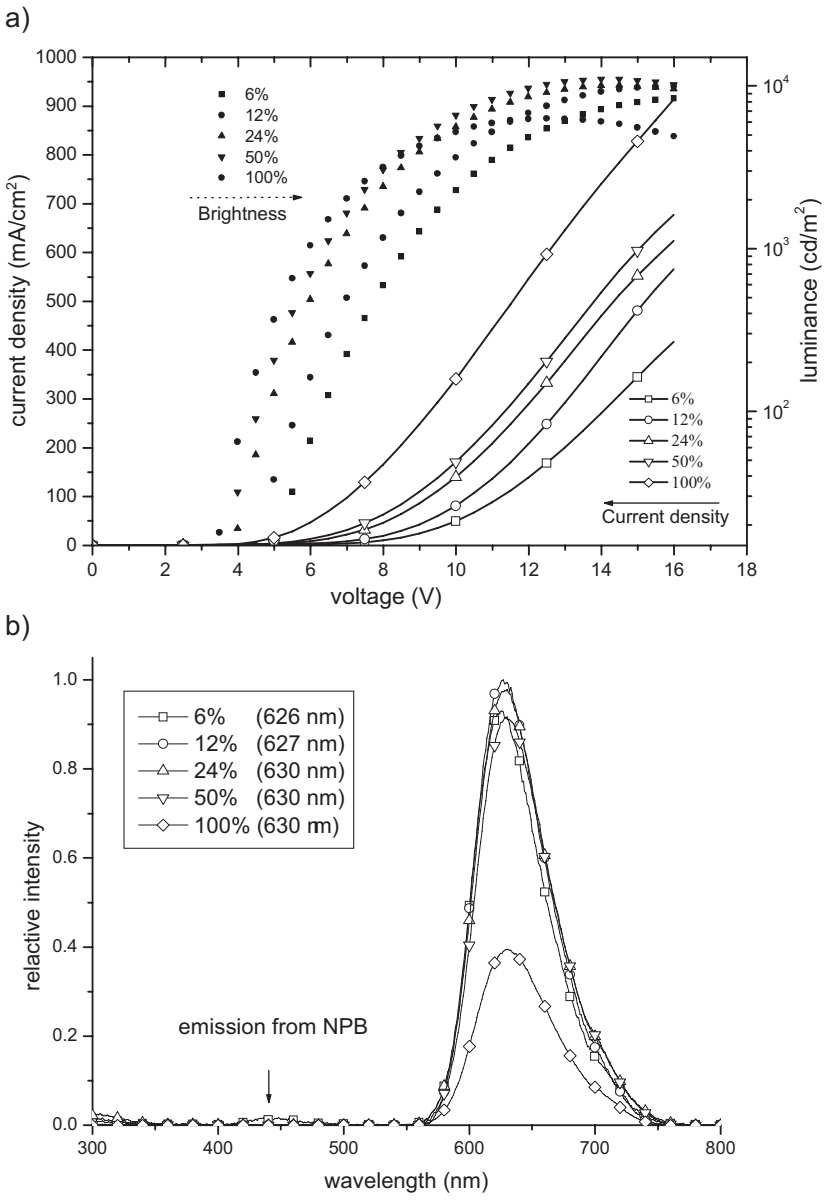

Figure 6. a) *I–V–L* characteristics of devices based on an ITO/NPB (40 nm)/CBP:X % **5**/BCP (10 nm)/AlQ_3 (30 nm)/Mg:Ag (10:1) configuration. b) EL spectra of the devices as a function of the doping concentration.

cence in solution, which is normally subject to a further spectral red-shift due to the polarization of the solvent. Nevertheless, the calculations qualitatively predict the relative arrangement of energy levels for these lower lying excited states.

For complex **3**, the lowest triplet state (T_1) mainly involves transitions from the HOMO to the lowest unoccupied molecular orbital (LUMO); the electron densities of the HOMO are located on the central metal atom and on the pyrazolate fragment of the chelating ligand, whereas those of the LUMO are essentially distributed over the entire isoquinoline moiety. The results clearly indicate that the lowest electronic $S_0 \rightarrow T_1$ transition is dominated by MLCT in combination with π–π* (intra-ligand charge transfer (ILCT); pyrazolate site (π) → isoqunioline site (π*)) transitions. This behavior is somewhat similar to $Ir(ppy)_3$ (ppy: 2-phenyl pyridine) and its derivatives, which are dominated primarily by a ^{3}π–π* transition, mixed to a great extent with ^{3}MLCT character.[28]

For cis complexes such as complex **6**, although the $S_0 \rightarrow T_1$ transition has a predominantly (ca. 60 %) MLCT character with some additional contribution from ILCT, there is a small but nonnegligible contribution from metal *d–d* transitions (see HOMO → LUMO + 1, Table 4 and Fig. 7), estimated to be around 3 % (Supporting Information). Moreover, formation of complexes **1** and **2** by substituting isoquinolyl pyrazolate with pyridyl pyrazolate further increases the $S_0 \rightarrow T_1$ energy gap. One thus expects a greater metal-centered *d–d* character in the $S_0 \rightarrow T_1$ transitions for these two molecules. This viewpoint is firmly supported by both spectral data and TDDFT calculations. As shown by the absorption spectra (Fig. 3), complex **2** apparently has the highest energy $S_0 \rightarrow T_1$ gap, and the theoretical peak λ_{max} is located at 482 nm. The results of TDDFT calculations (Fig. 7) of **2** also show that the T_1 state mainly has a metal *d–d* character (ca. 54 %, Supporting Information), while the typical ^{3}MLCT state has moved up in energy and become the second lowest excited state.

It is believed that the metal-centered *d–d* state possesses a very shallow potential well, which may undergo a surface crossing (i.e., a conical type of interception) with the S_0 state, inducing a dominant nonradiative pathway. Accordingly, this result implies that the deactivation of **2** occurs predominantly due to nonradiative processes, such as metal–ligand bond stretching motions. Experimental support for this is provided by the observation of a very weak emission for **2** in solid matrices at 77 K. On the other hand, complex **1**, coordinated with *tert*-butyl substituted chelates, exhibits weak but observable orange emission at room temperature (Table 2). This behavior arises from the electron-donating ability of the *tert*-butyl group, which makes the central metal atom more electron rich, resulting in the reduction of the $S_0 \rightarrow T_1$ gap. TDDFT calculations of **1** predict a $S_0 \rightarrow T_1$ transition at 510 nm, supporting this hypothesis. Furthermore, the *tert*-butyl substituents also reduce the metal *d–d* contribution to the T_1 state. The *d–d* contribution in **1** is approximately 30 %, as opposed to the approximately 54 % contribution in **2** (Supporting Information).

To further examine how far the $S_0 \rightarrow T_1$ energy gap can be tuned for this series of chelated Ru(II) complexes, we have conceptually designed complex **8** (Fig. 8), where only one pyrazolate chelate is used as the emitting chromophore. Note that the

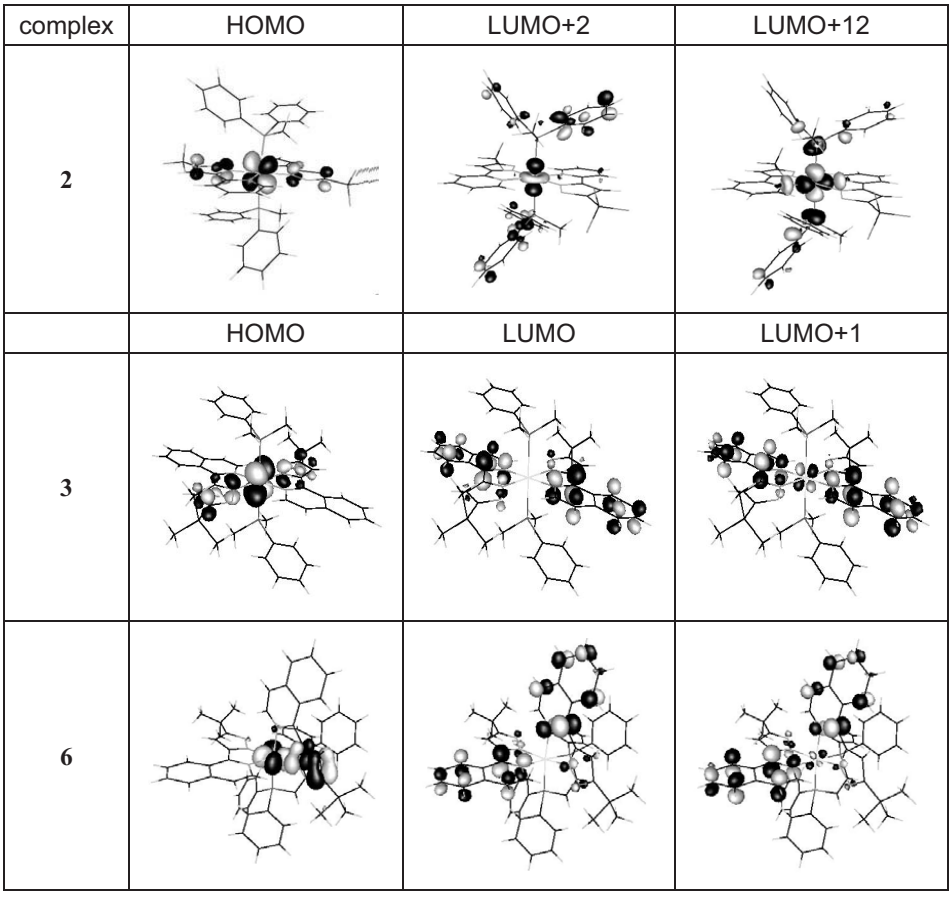

Figure 7. Selected frontier orbitals of **2**, **3**, and **6** involved in the lower lying transitions. Note that the contribution from LUMO + 4 for complex **2** is rather small and hence has been omitted.

Table 4. Calculated energy levels for the lower-lying transitions of **2**, **3**, and **6**.

		Assignments	[nm]	*E* [eV]	*F* [a]
2	T_1	HOMO → LUMO+2 (64%) HOMO → LUMO+4 (7%) HOMO → LUMO+12 (22%)	482	2.57	~0
3	T_1	HOMO → LUMO (+98%)	659.8	1.88	~0
	S_1	HOMO → LUMO+1 (+96%)	615.4	2.01	0.0107
6	T_1	HOMO → LUMO (+57%) HOMO → LUMO+1 (+29%) HOMO-2 → LUMO (5%)	559.3	2.22	~0
	S_1	HOMO → LUMO (+77%) HOMO-1 → LUMO (18%)	503.5	2.46	0.0081

[a] *F* = oscillator strength.

addition of a CF_3 substituent to the pyrazolate chelate in **8** is aimed at further stabilizing the HOMO level. A large ligand field splitting is also ensured by anchoring π-accepting ancillary ligands, such as CO and CN^{-1}, with the hope of shifting the metal *d*–*d* transitions to a higher energy, thereby ensuring that the π–π* transitions in the fppz ligand are again the lowest energy transitions.

As shown in Figure 8, the TDDFT calculation gives an expectedly large $S_0 \rightarrow T_1$ gap of approximately 2.91 eV (426 nm). Interestingly, analysis of the frontier orbitals shows that the d_π orbital no longer contributes to the HOMO. Accordingly, the $S_0 \rightarrow T_1$ transition is dominated by the intra-ligand $^3\pi$–π* transition, along with some excess ligand-to-metal charge transfer (LMCT) character. This causes a transfer of electron density to the metal d_{σ^*} orbitals, as well as to the π* orbitals of the ancillary ligands (Fig. 8). The population of metal d_{σ^*} orbitals and ancillary ligand π* orbitals will greatly weaken the internal bonding, providing a dominant non-radiative decay pathway for this hypothetical complex. Combining both experimental and theoretical results discussed in this section, we can safely conclude that the 482 nm absorption, i.e., the calculated energy gap of the $S_0 \rightarrow T_1$ transition for complex **2**, likely serves as an upper limit for these Ru(II) complexes, wherein they can avoid dominant metal *d*–*d* interference while still preserving an optimum emission efficiency.

3. Conclusions

Here, we have presented the rational design of a new series of luminescent charge-neutral ruthenium complexes, involving the utilization of isoquinolyl pyrazolate chromophores and a pair of phosphine ligands to produce an all trans coordination geometry. Complex **5** appears to be the most suitable candidate for OLED applications among this class of materials, showing bright saturated red emission in the solid state ($\lambda_{max} = 632$ nm and $\Phi = 0.24$). In contrast, the cis-substituted phosphine ligands show a significant hypsochromatic shift, which causes the emitting state to possess an increased proportion of metal *d*–*d* character, thereby leading to a drastic increase in the radiative lifetime as well as enhancing radiationless deactivation, thus reducing the quantum efficiency of these molecules. The worst scenario is therefore obtained using the least conjugated fppz and bppz ligands, which significantly increase the energy gap of all the transitions, resulting in a dominant metal-centered *d*–*d* character for the lowest triplet state.

Moreover, we have successfully obtained phosphorescent OLED devices based on these neutral Ru(II) complexes. It is believed that neutral complexes are better suited for OLED fabrication since their ionic counterparts tend to provide poor

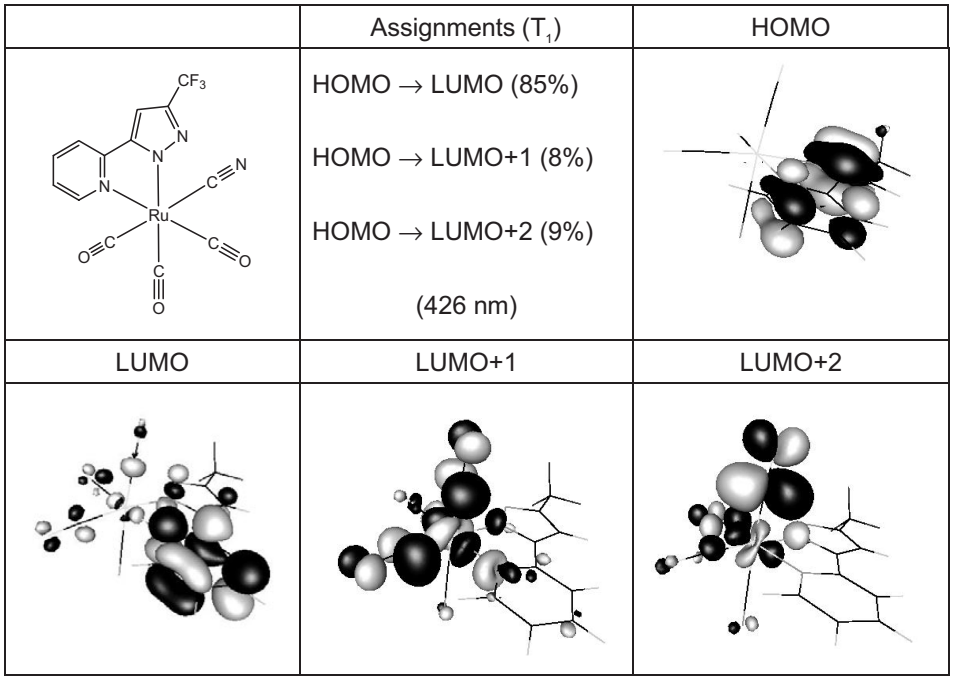

Figure 8. Proposed structure of **8**, along with its T_1 transition and the associated frontier orbitals.

control over the aggregation and spatial distribution of the charged constituents in the dopant matrix under an applied electric current. High efficiency and saturated red emission has been observed for devices employing complex **5** as a dopant, prepared by co-deposition with the CBP host. In contrast, the cis-oriented complex **6** produces an orange emitting device with somewhat inferior EL properties, a result attributed to its longer emission lifetime and relatively poor quantum efficiency.

Finally, we trust that this strategy for avoiding the incorporation of metal *d–d* character into the lowest triplet state will be equally applicable to other systems involving second-row transition metal elements. Most importantly, our results point out the competitive advantage of using charge-neutral Ru(II) emitters for manufacturing saturated red OLEDs. To the best of our knowledge, these results represent a major breakthrough in the development of phosphorescent OLEDs using less expensive second-row transition metal phosphors. We therefore believe that the results and prospects discussed in this study will spark a broad spectrum of interest in the field of photochemistry and OLED optoelectronics.

4. Experimental

General Information and Materials: Mass spectra (MS) were obtained on a JEOL SX-102A instrument operating in electron impact (EI) mode or fast atom bombardment (FAB) mode. ^{1}H and ^{13}C NMR spectra were recorded on Varian Mercury-400 and INOVA-500 instruments; chemical shifts (δ) for ^{1}H and ^{13}C NMR data are quoted in ppm with respect to the internal standard tetramethylsilane. Elemental analyses were carried out at the NSC Regional Instrumentation Center at National Chao Tung University, Hsinchu, Taiwan. An orange ruthenium complex [Ru(dpp=)(CO)$_3$] was synthesized by the reaction of $Ru_3(CO)_{12}$ and *cis*-1,2-bis-(diphenylphosphino)ethene under a CO atmosphere [29]. The pyrazole ligands, (bppz)H, (fppz)H, (ibpz)H, and (ifpz)H, were prepared according to literature procedures [30]. All other reactions were performed under a nitrogen atmosphere using anhydrous solvents or solvents treated with an appropriate drying reagent.

Preparation of ***1***: A 50 mL reaction flask was charged with (bppz)H (390 mg, 1.94 mmol), $Ru_3(CO)_{12}$ (200 mg, 0.31 mmol), and 20 mL of anhydrous diethylene glycol monoethyl ether (DGME). The mixture was heated at 160–170 °C for 24 h. The temperature was then lowered to approximately 120 °C, freshly sublimed Me_3NO (85 mg, 1.53 mmol) dissolved in 12 mL of DGME was added, and the mixture was stirred continuously for 5 min. Finally, PPh_2Me (840 μL, 4.50 mmol) was injected into the mixture. In the meantime, the temperature of the solution was raised to 180 °C. After 24 h, the reaction was stopped. The solvent was evaporated under vacuum, and the residue was washed with distilled water (20 mL × 2). Recrystallization was achieved by the slow diffusion of hexane vapor into a saturated ethyl acetate solution at room temperature, providing an orange crystalline solid (550 mg, 0.61 mmol) in 65 % yield. The yellow CF_3-substituted derivative complex **2** was prepared in 69 % yield using a similar procedure.

Spectral data for **1**: MS (FAB, ^{102}Ru): *m*/*z* 902 [M$^+$], 702 [M$^+$ – PPh_2Me], 502 [M$^+$ – 2PPh_2Me]. ^{1}H NMR (400 MHz, d_6-acetone): δ 10.35 (d, 2H, J_{HH} = 6.0 Hz), 7.18–7.13 (m, 6H), 7.06 (t, 2H, J_{HH} = 8.0 Hz), 7.02–6.94 (m, 6H), 6.87–6.79 (m, 6H), 6.67 (dt, 2H, J_{HH} = 6.0, 1.6 Hz), 6.61–6.59 (m, 4H), 6.27 (s, 2H), 1.58 (s, 18H, ^{t}Bu), 1.04 (t, 6H, J_{HP} = 2.8 Hz, Me). ^{31}P NMR (202 MHz, d_6-acetone): δ –19.6 (s). Anal. Calcd. for $C_{50}H_{54}N_6P_2Ru$: C, 66.58; N, 9.32; H, 6.03. Found: C, 66.56; N, 9.28; H, 6.01.

Spectral data for **2**: MS (FAB, ^{102}Ru): *m*/*z* 926 [M$^+$], 726 [M$^+$ – PPh_2Me], 526 [M$^+$ – 2PPh_2Me]. ^{1}H NMR (400 MHz, d_6-acetone): δ 10.28 (d, 2H, J_{HH} = 5.8 Hz), 7.41 (t, 2H, J_{HH} = 7.8 Hz), 7.12–7.05 (m, 6H), 7.01 (ddd, 2H, J_{HH} = 5.8, 7.0, 1.6 Hz), 6.96 (t, 4H, J_{HH} = 7.8 Hz), 6.93–6.86 (m, 8H), 6.78 (s, 2H), 6.68–6.64 (m, 4H), 1.14 (t, 6H, J_{HP} = 3.0 Hz, Me). ^{31}P NMR (242 MHz, d_6-acetone): δ 16.6 (s). Anal. Calcd. for $C_{44}H_{36}F_6N_6P_2Ru$: C, 57.08; N, 9.08; H, 3.92. Found: C, 57.14; N, 9.18; H, 4.04.

Preparation of Isoquinolyl Complexes ***3***, ***4***, *and* ***5***: The synthetic procedures used were essentially identical to those for **1**, using similar ratios of (ibpz)H or (ifpz)H, $Ru_3(CO)_{12}$, freshly sublimed Me_3NO, and phosphine ligands such as $PPhMe_2$ or PPh_2Me. Red complexes **3**, **4**, and **5** were obtained in 62 %, 61 %, and 63 % yields, respectively.

Spectral Data for **3**: MS (FAB, ^{102}Ru): *m*/*z* 878 [M$^+$], 740 [M$^+$ – $PPhMe_2$], 602 [M$^+$ – 2$PPhMe_2$]. ^{1}H NMR (400 MHz, C_6D_6): δ 10.83 (d, 2H, J_{HH} = 6.8 Hz), 8.76 (d, 2H, J_{HH} = 7.2 Hz), 7.40 (d, 2H, J_{HH} = 6.8 Hz), 7.24–7.23 (m, 4H), 7.20 (s, 2H), 6.91 (d, 2H, J_{HH} = 6.4 Hz), 6.62–6.55 (m, 6H), 6.50–6.47 (m, 6H), 1.88 (s, 18H, ^{t}Bu), 0.70 (t, 6H, J_{HP} = 3.1 Hz, Me), 0.44 (t, 6H, J_{HP} = 3.1 Hz, Me). ^{31}P NMR (202 MHz, C_6D_6): δ 12.3 (s). Anal. Calcd for $C_{48}H_{54}N_6P_2Ru$: C, 65.66; N, 9.57; H, 6.20. Found: C, 65.20; N, 9.33; H, 6.24.

Spectral Data for **4**: MS (FAB, ^{102}Ru): *m*/*z* 1003 [M$^+$], 803 [M$^+$ – PPh_2Me], 603 [M$^+$ – 2PPh_2Me]. ^{1}H NMR (400 MHz, d_6-acetone): δ 10.75 (d, 2H, J_{HH} = 7.0 Hz), 8.39 (d, 2H, J_{HH} = 8.4 Hz), 7.69 (d, 2H, J_{HH} = 7.0 Hz), 7.53–7.43 (m, 4H), 7.18 (d, 2H, J_{HH} = 6.8 Hz), 7.09–7.05 (m, 4H), 6.89 (s, 2H), 6.86–6.77 (m, 6H), 6.72 (t, 2H, J_{HH} = 7.2 Hz),

6.60–6.51 (m, 8 H), 1.69 (s, 18 H, ^{t}Bu), 1.06 (t, 6 H, J_{HP} = 3.0 Hz, Me). ^{31}P NMR (242 MHz, d_6-acetone): δ 18.0 (s). Anal. Calcd for $C_{58}H_{58}N_6P_2Ru$: C, 69.51; N, 8.39; H, 5.83. Found: C, 69.55; N, 8.67; H, 6.09.

Spectral Data for **5**: MS (FAB, ^{102}Ru): *m*/*z* 1026 [M$^+$], 826 [M$^+$ – PPh$_2$Me], 626 [M$^+$ – 2PPh$_2$Me]. ^{1}H NMR (400 MHz, d_6-acetone): δ 10.62 (d, 2 H, J_{HH} = 6.4 Hz), 8.33 (d, 2 H, J_{HH} = 7.6 Hz), 7.85 (d, 2 H, J_{HH} = 7.7 Hz), 7.65 (dd, 2 H, J_{HH} = 6.8, 7.6 Hz), 7.57 (dd, 2 H, J_{HH} = 7.7, 6.8 Hz), 7.52 (d, 2 H, J_{HH} = 6.4 Hz), 7.36 (s, 2 H), 6.85–6.80 (m, 8 H), 6.77–6.75 (m, 4 H), 6.69–6.63 (m, 8 H), 1.82 (t, 6 H, J_{HP} = 3.0 Hz, Me). ^{19}F NMR (470 MHz, d_6-acetone): δ –59.1 (s, CF_3). ^{31}P NMR (202 MHz, d_6-acetone): δ 15.7 (s). Anal. Calcd for $C_{52}H_{40}F_6N_6P_2Ru$: C, 60.88; N, 8.19; H, 3.93. Found: C, 60.88; N, 8.10; H, 4.04.

Preparation of **6**: To a 50 mL reaction flask was added [Ru(dpp=)(CO)$_3$] (757 mg, 1.30 mmol), (ibpz)H (685 mg, 2.72 mmol), and 20 mL of anhydrous DGME solvent. The mixture was heated at 170–180 °C for a period of 24 h. Subsequently, the solution was evaporated to dryness and the residue was purified by recrystallization from a saturated ethyl acetate solution, giving a red crystalline solid (765 mg, 0.77 mmol) in 59 % yield. The related orange complex **7** was obtained in 61 % yield by following similar procedures.

Spectral Data for **6**: MS (FAB, ^{102}Ru): *m*/*z* 998 [M$^+$], 747 [M$^+$ – ibpz], 498 [M$^+$ – 2ibpz]. ^{1}H NMR (500 MHz, d_6-acetone): δ 8.55 (d, 2 H, J_{HH} = 7.5 Hz), 8.06 (t, 4 H, J_{HH} = 9.0 Hz), 7.87–7.75 (m, 2 H), 7.62 (d, 2 H, J_{HH} = 7.5 Hz), 7.56 (dt, 2 H, J_{HH} = 8.5, 1.0 Hz), 7.51 (dt, 2 H, J_{HH} = 8.5, 1.0 Hz), 7.30 (t, 2 H, J_{HH} = 7.0 Hz), 7.18 (t, 4 H, J_{HH} = 7.0 Hz), 6.94 (dd, 2 H, J_{HH} = 8.0, 2.0 Hz), 6.91–6.86 (m, 4 H), 6.83 (s, 2 H), 6.79 (t, 4 H, J_{HH} = 8.0 Hz), 6.66 (t, 4 H, J_{HH} = 7.0 Hz), 1.53 (s, 18 H, ^{t}Bu). ^{31}P NMR (202 MHz, d_6-acetone): δ 72.4 (s). Anal. Calcd. for $C_{58}H_{54}N_6P_2Ru$: C, 69.79; N, 8.42; H, 5.45. Found: C, 70.23; N, 8.43; H, 5.39.

Spectral Data for **7**: MS (FAB, ^{102}Ru): *m*/z 1022 [M$^+$], 759 [M$^+$ – ifpz], 496 [M$^+$ – 2ifpz]. ^{1}H NMR (500 MHz, d_6-acetone): δ 8.57 (d, 2 H, J_{HH} = 8.5 Hz), 8.03–7.91 (m, 2 H), 7.88 (t, 4 H, J_{HH} = 9.5 Hz), 7.75 (dd, 2 H, J_{HH} = 7.0, 2.0 Hz), 7.69–7.63 (m, 4 H), 7.35 (t, 2 H, J_{HH} = 7.5 Hz), 7.33 (s, 2 H), 7.22–7.20 (m, 6 H), 7.00 (dd, 2 H, J_{HH} = 6.0, 1.5 Hz), 6.95 (dt, 2 H, J_{HH} = 7.0, 1.0 Hz), 6.70–6.63 (m, 8 H). ^{19}F NMR (470 MHz, d_6-acetone): δ –59.5 (s). ^{31}P NMR (242 MHz, d_6-acetone): δ 72.3 (s). Anal. Calcd. for $C_{52}H_{36}F_6N_6P_2Ru$: C, 61.12; N, 8.22; H, 3.55. Found: C, 61.31; N, 8.60; H, 3.90.

X-ray Diffraction Studies: Single crystal X-ray diffraction data was obtained on a Bruker SMART Apex charge coupled device (CCD) diffractometer using (Mo Kα) radiation (λ = 0.71073 Å). The data was collected using the SMART program. Cell refinement and data reduction were performed with the SAINT program. The structure was determined using the SHELXTL/PC program and refined using full-matrix least squares. Crystallographic refinement parameters for complexes **3** and **6** are summarized in Table 1. Their crystallographic data (excluding structure factors) have been deposited in the Cambridge Crystallographic Data Centre with deposition numbers CCDC-261 543 and CCDC-298 979, respectively. This data can be obtained free of charge on application to CCDC, 12 Union Road, Cambridge CB21EZ (UK) (fax: (+44) 1223-336-033; E-mail: deposit@ccdc.cam.ac.uk).

Electrochemical Measurements: Cyclic voltammetry (CV) measurements were performed using a BAS 100 B/W electrochemical analyzer. The oxidation and reduction measurements were recorded using Pt wire and Au disks coated with Hg as the working electrodes, respectively. The measurements were made in anhydrous CH_2Cl_2 and THF solution containing 0.1 M $TBAPF_6$ as the supporting electrolyte with a typical scan rate of 100 mV s^{-1}. The potentials were measured against a Ag/Ag$^+$ (0.01 M $AgNO_3$) reference electrode with ferrocene as the internal standard.

Photophysical Data Measurement and OLED Fabrication: Steady-state absorption, emission, and phosphorescence lifetime measurements, both in solution and in the solid state, have been described in our previous reports [31]. For measuring quantum yields in the solid state, an integrating sphere (Labsphere) was used. The solid film was prepared via a vapor deposition method and was excited by a 514 nm Ar^+ laser line. The emission was then acquired by an intensified CCD for subsequent analyses [32]. The fabrication procedures for the OLEDs, including for patterning and cleaning the ITO substrates, followed methods previously described in the literature [27].

Theoretical Calculations: TDDFT [33] calculations using B3LYP [34] functions were performed based on the structures obtained from single crystal X-ray diffraction. A "Double-ζ" quality basis set consisting of Hay and Wadt's effective core potentials (LANL2DZ) [35] was used for the Ru atom and 6-31G* basis sets were used for H, C, N, and P atoms [36]. A relativistic effective core potential (ECP) was used to replace the inner core electrons of Ru(II), leaving the outer core ($4s^24p^6$) electrons and the $4d^6$ valence electrons. Typically, the lowest ten triplet and ten singlet roots of the non-Hermitian eigenvalue equations were obtained to determine the vertical excitation energies. Oscillator strengths were deduced from the dipole transition matrix elements (for singlet states only). The excited-state TDDFT calculations were carried out using Gaussian03 as described in our previous publication [37].

Received: December 14, 2005
Final version: March 3, 2006

[1] C. W. Tang, S. A. Vanslyke, *Appl. Phys. Lett.* **1987**, *51*, 913.
[2] U. Mitschke, P. Bauerle, *J. Mater. Chem.* **2000**, *10*, 1471.
[3] a) C. Adachi, M. A. Baldo, S. R. Forrest, S. Lamansky, M. E. Thompson, R. C. Kwong, *Appl. Phys. Lett.* **2001**, *78*, 1622. b) A. Tsuboyama, H. Iwawaki, M. Furugori, T. Mukaide, J. Kamatani, S. Igawa, T. Moriyama, S. Miura, T. Takiguchi, S. Okada, M. Hoshino, K. Ueno, *J. Am. Chem. Soc.* **2003**, *125*, 12 971. c) C. Jiang, W. Yang, J. Peng, S. Xiao, Y. Cao, *Adv. Mater.* **2004**, *16*, 537.
[4] a) Y.-L. Tung, S.-W. Lee, Y. Chi, Y.-T. Tao, C.-H. Chien, Y.-M. Cheng, P.-T. Chou, S.-M. Peng, C.-S. Liu, *J. Mater. Chem.* **2005**, *15*, 460. b) X. Jiang, A. K. Y. Jen, B. Carlson, L. R. Dalton, *Appl. Phys. Lett.* **2002**, *81*, 3125. c) B. Carlson, G. D. Phelan, W. Kaminsky, L. Dalton, X. Z. Jiang, S. Liu, A. K. Y. Jen, *J. Am. Chem. Soc.* **2002**, *124*, 14 162. d) S. Bernhard, X. Gao, G. G. Malliaras, H. D. Abruna, *Adv. Mater.* **2002**, *14*, 433. e) Y. Ma, H. Zhang, J. Shen, C. Che, *Synth. Met.* **1998**, *94*, 245.
[5] a) F.-M. Hwang, H.-Y. Chen, P.-S. Chen, C.-S. Chi, Y. Liu, C.-F. Shu, F.-I. Wu, P.-T. Chou, S.-M. Peng, G.-H. Lee, *Inorg. Chem.* **2005**, *44*, 1344. b) Y.-H. Niu, B. Chen, S. Liu, H. Yip, J. Bardecker, A. K. Y. Jen, J. Kavitha, Y. Chi, C.-F. Shu, Y.-H. Tseng, C.-H. Chien, *Appl. Phys. Lett.* **2004**, *85*, 1619. c) X. Gong, S.-H. Lim, J. C. Ostrowski, D. Moses, C. J. Bardeen, G. C. Bazan, *J. Appl. Phys.* **2004**, *95*, 948. d) X. Chen, J.-L. Liao, Y. Liang, M. O. Ahmed, H. E. Tseng, S. A. Chen, *J. Am. Chem. Soc.* **2003**, *125*, 636. e) S. Lamansky, P. Djurovich, D. Murphy, F. Abdel-Razzaq, H.-E. Lee, C. Adachi, P. E. Burrows, S. R. Forrest, M. E. Thompson, *J. Am. Chem. Soc.* **2001**, *123*, 4304.
[6] a) S.-Y. Chang, J. Kavitha, S.-W. Li, C.-S. Hsu, Y. Chi, Y.-S. Yeh, P.-T. Chou, G.-H. Lee, A. J. Carty, Y.-T. Tao, C.-H. Chien, *Inorg. Chem.* **2006**, *45*, 137. b) W. Lu, B.-X. Mi, M. C. W. Chan, Z. Hui, C.-M. Che, N. Zhu, S.-T. Lee, *J. Am. Chem. Soc.* **2004**, *126*, 4958. c) C.-M. Che, Y.-J. Hou, M. C. W. Chan, J. Guo, Y. Liu, Y. Wang, *J. Mater. Chem.* **2003**, *13*, 1362. d) J. Brooks, Y. Babayan, S. Lamansky, P. I. Djurovich, I. Tsyba, R. Bau, M. E. Thompson, *Inorg. Chem.* **2002**, *41*, 3055.
[7] a) C. Adachi, M. A. Baldo, M. E. Thompson, S. R. Forrest, *J. Appl. Phys.* **2001**, *90*, 5048. b) Y. Kawamura, K. Goushi, J. Brooks, J. J. Brown, H. Sasabe, C. Adachi, *Appl. Phys. Lett.* **2005**, *86*, 071 104.
[8] a) C. H. Lyons, E. D. Abbas, J.-K. Lee, M. F. Rubner, *J. Am. Chem. Soc.* **1998**, *120*, 12 100. b) M. Buda, G. Kalyuzhny, A. J. Bard, *J. Am. Chem. Soc.* **2002**, *124*, 6090. c) F. G. Gao, A. J. Bard, *Chem. Mater.* **2002**, *14*, 3465. d) S. Bernhard, J. A. Barron, P. L. Houston, H. D. Abruna, J. L. Ruglovksy, X. Gao, G. G. Malliaras, *J. Am. Chem. Soc.* **2002**, *124*, 13 624. e) H.-J. Su, F.-I. Wu, C.-F. Shu, Y.-L. Tung, Y. Chi, G.-H. Lee, *J. Polym. Sci., Part A: Polym. Chem.* **2005**, *43*, 859.
[9] a) G. Kalyuzhny, M. Buda, J. McNeill, P. Barbara, A. J. Bard, *J. Am. Chem. Soc.* **2003**, *125*, 6272. b) H. Rudmann, S. Shimada, M. F. Rubner, *J. Appl. Phys.* **2003**, *94*, 115. c) C.-Y. Liu, A. J. Bard, *J. Am. Chem. Soc.* **2002**, *124*, 4190. d) H. Rudmann, S. Shimada, M. F. Rubner, *J.*

Am. Chem. Soc. **2002**, *124*, 4918. e) H. Rudmann, M. F. Rubner, *J. Appl. Phys.* **2001**, *90*, 4338. f) E. Holder, B. M. W. Langeveld, U. S. Schubert, *Adv. Mater.* **2005**, *17*, 1109.

[10] a) S. Welter, K. Brunner, J. W. Hofstraat, L. De Cola, *Nature* **2003**, *421*, 54. b) J. D. Slinker, A. A. Gorodetsky, M. S. Lowry, J. Wang, S. Parker, R. Rohl, S. Bernhard, G. G. Malliaras, *J. Am. Chem. Soc.* **2004**, *126*, 2763. c) D. A. Bernards, J. D. Slinker, G. G. Malliaras, S. Flores-Torres, H. D. Abruna, *Appl. Phys. Lett.* **2004**, *84*, 4980. d) D. Dini, *Chem. Mater.* **2005**, *17*, 1933.

[11] a) H. Xia, C. Zhang, X. Liu, S. Qiu, P. Lu, F. Shen, J. Zhang, Y. Ma, *J. Phys. Chem. B* **2004**, *108*, 3185. b) H. Xia, C. Zhang, S. Qiu, P. Lu, J. Zhang, Y. Ma, *Appl. Phys. Lett.* **2004**, *84*, 290. c) J. Yang, K. C. Gordon, *Chem. Phys. Lett.* **2003**, *372*, 577. d) J. Yang, K. C. Gordon, *Chem. Phys. Lett.* **2004**, *385*, 481.

[12] Y.-L. Tung, S.-W. Lee, Y. Chi, L.-S. Chen, C.-F. Shu, F.-I. Wu, A. J. Carty, P.-T. Chou, S.-M. Peng, G.-H. Lee, *Adv. Mater.* **2005**, *17*, 1059.

[13] a) S. Zalis, I. R. Farrell, A. Vlcek Jr., *J. Am. Chem. Soc.* **2003**, *125*, 4580. b) M. K. Nazeeruddin, R. Humphry-Baker, D. Berner, S. Rivier, L. Zuppiroli, M. Graetzel, *J. Am. Chem. Soc.* **2003**, *125*, 8790.

[14] a) C.-C. Cheng, W.-S. Yu, P.-T. Chou, S.-M. Peng, G.-H. Lee, P.-C. Wu, Y.-H. Song, Y. Chi, *Chem. Commun.* **2003**, 2628. b) H.-Y. Chen, Y. Chi, C.-S. Liu, J.-K. Yu, Y.-M. Cheng, K.-S. Chen, P.-T. Chou, S.-M. Peng, G.-H. Lee, A. J. Carty, S.-J. Yeh, C.-T. Chen, *Adv. Funct. Mater.* **2005**, *15*, 567.

[15] J. Kavitha, S.-Y. Chang, Y. Chi, J.-K. Yu, Y.-H. Hu, P.-T. Chou, S.-M. Peng, G.-H. Lee, Y.-T. Tao, C.-H. Chien, A. J. Carty, *Adv. Funct. Mater.* **2004**, *15*, 223.

[16] a) J.-K. Yu, Y.-H. Hu, Y.-M. Cheng, P.-T. Chou, S.-M. Peng, G.-H. Lee, A. J. Carty, Y.-L. Tung, S.-W. Lee, Y. Chi, C.-S. Liu, *Chem. Eur. J.* **2004**, *10*, 6255. b) P.-C. Wu, J.-K. Yu, Y.-H. Song, Y. Chi, P.-T. Chou, S.-M. Peng, G.-H. Lee, *Organometallics* **2003**, *22*, 4938.

[17] Y.-L. Tung, P.-C. Wu, C.-S. Liu, Y. Chi, J.-K. Yu, Y.-H. Hu, P.-T. Chou, S.-M. Peng, G.-H. Lee, Y. Tao, A. J. Carty, C.-F. Shu, F.-I. Wu, *Organometallics* **2004**, *23*, 3745.

[18] a) A. El-Ghayoury, A. Harriman, A. Khatyr, R. Ziessel, *Angew. Chem. Int. Ed.* **2000**, *39*, 185. b) P. A. Anderson, F. R. Keene, T. J. Meyer, J. A. Moss, G. F. Strouse, J. A. Treadway, *J. Chem. Soc., Dalton Trans.* **2002**, 3820. c) Y.-Q. Fang, N. J. Taylor, G. S. Hanan, F. Loiseau, R. Passalacqua, S. Campagna, H. Nierengarten, A. Van Dorsselaer, *J. Am. Chem. Soc.* **2002**, *124*, 7912.

[19] a) D. P. Rillema, D. S. Jones, H. A. Levy, *J. Chem. Soc., Chem. Commun.* **1979**, 849. b) B. M. Golstein, J. K. Barton, H. M. Berman, *Inorg. Chem.* **1986**, *25*, 842. c) P. A. Anderson, G. B. Deacon, K. H. Haarmann, F. R. Keene, T. J. Meyer, D. A. Reitsma, B. W. Skelton, G. F. Strouse, N. C. Thomas, J. A. Treadway, A. H. White, *Inorg. Chem.* **1995**, *34*, 6145. d) C. M. Kepert, A. M. Bond, G. B. Deacon, L. Spiccia, B. W. Skelton, A. H. White, *J. Chem. Soc., Dalton Trans.* **2004**, 1766.

[20] A. Vlcek Jr., *Coord. Chem. Rev.* **1998**, *177*, 219.

[21] a) W.-S. Huang, J. T. Lin, C.-H. Chien, Y.-T. Tao, S.-S. Sun, Y.-S. Wen, *Chem. Mater.* **2004**, *16*, 2480. b) S. Lamansky, P. Djurovich, D. Murphy, F. Abdel-Razzaq, R. Kwong, I. Tsyba, M. Bortz, B. Mui, R. Bau, M. E. Thompson, *Inorg. Chem.* **2001**, *40*, 1704.

[22] C. Adachi, M. A. Baldo, S. R. Forrest, M. E. Thompson, *Appl. Phys. Lett.* **2000**, *77*, 904.

[23] a) Y.-Y. Noh, C.-L. Lee, J.-J. Kim, *J. Chem. Phys.* **2003**, *118*, 2853. b) R. J. Holmes, B. W. D'Andrade, S. R. Forrest, X. Ren, J. Li, M. E. Thompson, *Appl. Phys. Lett.* **2003**, *83*, 3818.

[24] V. Bulovic, R. Deshpande, M. E. Thompson, S. R. Forrest, *Chem. Phys. Lett.* **1999**, *308*, 317.

[25] a) F.-C. Chen, C.-W. Chu, J. He, Y. Yang, J.-L. Lin, *Appl. Phys. Lett.* **2004**, *85*, 3295. b) T. M. Brown, J. S. Kim, R. H. Friend, F. Cacialli, R. Daik, W. J. Feast, *Appl. Phys. Lett.* **1999**, *75*, 1679.

[26] a) J. L. Kim, J. K. Kim, H. N. Cho, D. Y. Kim, C. Y. Kim, S. I. Hong, *Macromolecules* **2000**, *33*, 5880. b) X. W. Zhan, Y. Q. Liu, X. Wu, S. A. Wang, D. B. Zhu, *Macromolecules* **2002**, *35*, 2529. c) C. J. Tonzola, M. M. Alam, B. A. Bean, S. A. Jenekhe, *Macromolecules* **2004**, *37*, 3554.

[27] Y.-H. Song, S.-J. Yeh, C.-T. Chen, Y. Chi, C.-S. Liu, J.-K. Yu, Y.-H. Hu, P.-T. Chou, S.-M. Peng, G.-H. Lee, *Adv. Funct. Mater.* **2004**, *14*, 1221.

[28] P. J. Hay, *J. Phys. Chem. A* **2002**, *106*, 1634.

[29] S.-J. Skoog, A.-L. Jorgenson, J.-P. Campbell, M.-L. Douskey, E. Munson, W.-L. Gladfelter, *J. Organomet. Chem.* **1998**, *557*, 13.

[30] a) S. Kubota, M. Uda, T. Nakagawa, *J. Heterocycl. Chem.* **1975**, *12*, 855. b) K. Funabiki, N. Noma, G. Kuzuya, M. Matsui, K. Shibata, *J. Chem. Res., Synop.* **1999**, 1301.

[31] P.-T. Chou, W.-S. Yu, Y.-M. Cheng, S.-C. Pu, Y.-C. Yu, Y.-C. Lin, C.-H. Huang, C.-T. Chen, *J. Phys. Chem. A* **2004**, *108*, 6487.

[32] J. C. De Mello, F. H. Wittmann, R. H. Friend, *Adv. Mater.* **1997**, *9*, 230.

[33] a) C. Jamorski, M. E. Casida, D. R. Salahub, *J. Chem. Phys.* **1996**, *104*, 5134. b) M. Petersilka, U. J. Grossmann, E. K. U. Gross, *Phys. Rev. Lett.* **1996**, *76*, 1212. c) R. Bauernschmitt, R. Ahlrichs, F. H. Hennrich, M. M. Kappes, *J. Am. Chem. Soc.* **1998**, *120*, 5052. d) M. E. Casida, *J. Chem. Phys.* **1998**, *108*, 4439. e) R. E. Stratmann, G. E. Scuseria, M. J. Frisch, *J. Chem. Phys.* **1998**, *109*, 8218.

[34] a) C. Lee, W. Yang, R. G. Parr, *Phys. Rev. B: Condens. Matter* **1988**, *37*, 785. b) A. D. Becke, *J. Chem. Phys.* **1993**, *98*, 5648.

[35] a) P. J. Hay, W. R. Wadt, *J. Chem. Phys.* **1985**, *82*, 270. b) W. R. Wadt, P. J. Hay, *J. Chem. Phys.* **1985**, *82*, 284. c) P. J. Hay, W. R. Wadt, *J. Chem. Phys.* **1985**, *82*, 299.

[36] P. C. Hariharan, J. A. Pople, *Mol. Phys.* **1974**, *27*, 209.

[37] J.-K. Yu, Y.-M. Cheng, Y.-H. Hu, P.-T. Chou, Y.-L. Chen, S.-W. Lee, Y. Chi, *J. Phys. Chem. B* **2004**, *108*, 19 908.